# High-Performance All-Solid-State Proton Rectifier Using a Heterogeneous Membrane Composed of Coordination Polymer and Layered Double Hydroxide

Jiangfeng Lu, Yukihiro Yoshida*, Mitsuhiko Maesato, Hiroshi Kitagawa*

[*] Jiangfeng Lu, Prof. Yukihiro Yoshida, Prof. Mitsuhiko Maesato, Prof. Hiroshi Kitagawa
Division of Chemistry, Graduate School of Science, Kyoto University, Kitashirakawa-Oiwakecho, Sakyo-ku, Kyoto 606-8502(Japan)
E-mail: yoshiday@kuchem.kyoto-u.ac.jp; kitagawa@kuchem.kyoto-u.ac.jp

Supporting information for this article is given via a link at the end of the document.

**Abstract:** Rational control of unidirectional proton transport is highly challenging, primarily owing to the difficulty in introducing an asymmetric factor into proton conducting media. In this study, free-standing membranes of a proton-conducting two-dimensional porous coordination polymer, $Cu_2$(CuTCPP) ($H_2$TCPP: 5,10,15,20-tetrakis(4-carboxyphenyl)porphyrin) and a hydroxide ion-conducting layered double hydroxide, Mg-Al-LDH($NO_3$), were combined to generate a pH gradient in the conducting media. The current–voltage measurements revealed that the heterogeneous membrane exhibits a significant unidirectional proton transport with a proton rectification ratio exceeding 200 under 90% relative humidity in the initial voltage scan. This value is the highest among the reported all-solid-state proton rectifiers. The high designability of both components with well-defined structures, which is in contrast to the organic polymers used so far, provides a new avenue for developing and understanding the proton-rectifying behavior in the solid state.

## Introduction

Unidirectional proton transport plays an essential role in adenosine triphosphate production, which is driven by the pH gradient generated by proton pumps across cell membranes.[1] It is also critical for developing various artificial systems such as artificial photosynthesis,[2] electrodialysis technology,[3] and proton exchange fuel cells.[4] However, introducing at least one asymmetric factor into the proton pathway (e.g., spatial structure, surface potential, and electrolyte media[5]) is the most serious obstacle to achieving the unidirectional proton transport. A simple and practical example is the combination of cation- and anion-exchange membranes to impose a pH gradient, as applied in the first study on a liquid electrolyte-based proton rectifier device.[6] The device structure is best described by an electrolytic analogy with p–n diode, wherein protons and hydroxide ions are the dominant carrier species instead of electrons and holes. Specifically, an asymmetric surface potential is introduced to promote ion diffusion driven by the concentration gradient.[7] As subsequently discussed in detail, the pH gradient directs the diffusion current of protons/hydroxide ions toward the interfacial region, which is balanced by the drift current flowing in the opposite direction under no applied voltage (Figure 1a). Application of a forward bias voltage explicitly promotes both proton and hydroxide ion diffusions, which is primarily associated with the decrease in the potential barrier (so-called built-in potential). In contrast, the reverse bias voltage suppresses the diffusions due to the increased potential barrier.

Compared to the liquid electrolyte-based proton rectifier devices,[5, 8] the fabrication of all-solid-state devices remains in the nascent stage[9] despite their apparent advantages of thin configuration, high flexibility, and high safety against liquid leakage. In addition, the components of membranes in all-solid-state proton rectifiers have been limited to amorphous organic polymers with low designability, leading to the difficulty in studying the rectifying behavior from a structural perspective. To overcome these drawbacks, we adopted structurally defined porous coordination polymers (PCPs)[10] as proton conductors[11]. The high designability of PCPs, which primarily originates from their diverse combinations of metal nodes and organic linkers, enables rational control of porous structures with tunable sizes, topologies, and surface potentials.[12] In particular, PCPs with high proton conduction have been extensively investigated by judicious selection of the components, wherein water molecules included in the pores serve as proton hopping sites.[13] However, unidirectional proton transport has been largely unexplored in PCP systems; to date, no PCP-based all-solid-state proton rectifiers capable of preventing liquid leakage have been fabricated. We selected $Cu_2$(CuTCPP) ($H_4$($H_2$TCPP); 5,10,15,20-tetrakis(4-carboxyphenyl)porphyrin) with a two-dimensional (2D) square grid structure composed of copper porphyrins and paddlewheel-type copper dimers (Figure 1b),[14] because it exhibits a high in-plane proton conductivity ($3.9 \times 10^{-3}$ S cm$^{-1}$ at 25 °C under 98% relative humidity (RH)) and can be assembled into 2D nanosheets.[15] The moderate intersheet interaction mainly through van der Waals force provides considerable freedom in the stacking manner, which favors the formation of a free-standing mem-brane.[16] As a hydroxide ion conductor, Mg-Al layered double hydroxide (LDH), with 2D layers composed of edge-shared Mg(II) and Al(III) hydroxide octahedra (Figure 1c),[17] was selected, because the in-plane hydroxide ion conductivity ($1 \times 10^{-1}$ S cm$^{-1}$ at 60 °C under 80% RH) is among the highest reported to date, and the 2D layers can be readily exfoliated into nanosheets, as in $Cu_2$(CuTCPP).[18] Theoretical calculations predicted that guest water molecules energetically prefer to transfer protons to immobile hydroxyl sites in Mg-Al-LDH layers to generate mobile $OH^-$ ions ($M(OH)_2 + xH_2O \leftrightarrow M(H_2O)_x(OH)_{2-x}^{x+} + xOH^-$; Figure S1).[19] In this study, free-standing membranes of each ion conductor were separately prepared, followed by the mechanical fabrication of their heterogeneous membrane, which was sandwiched by Pd electrodes. The electrodes can serve as proton transmission media and catalysts for water dissociation, as discussed subsequently. Particularly, both components with layered structures can adsorb a considerable amount of water,

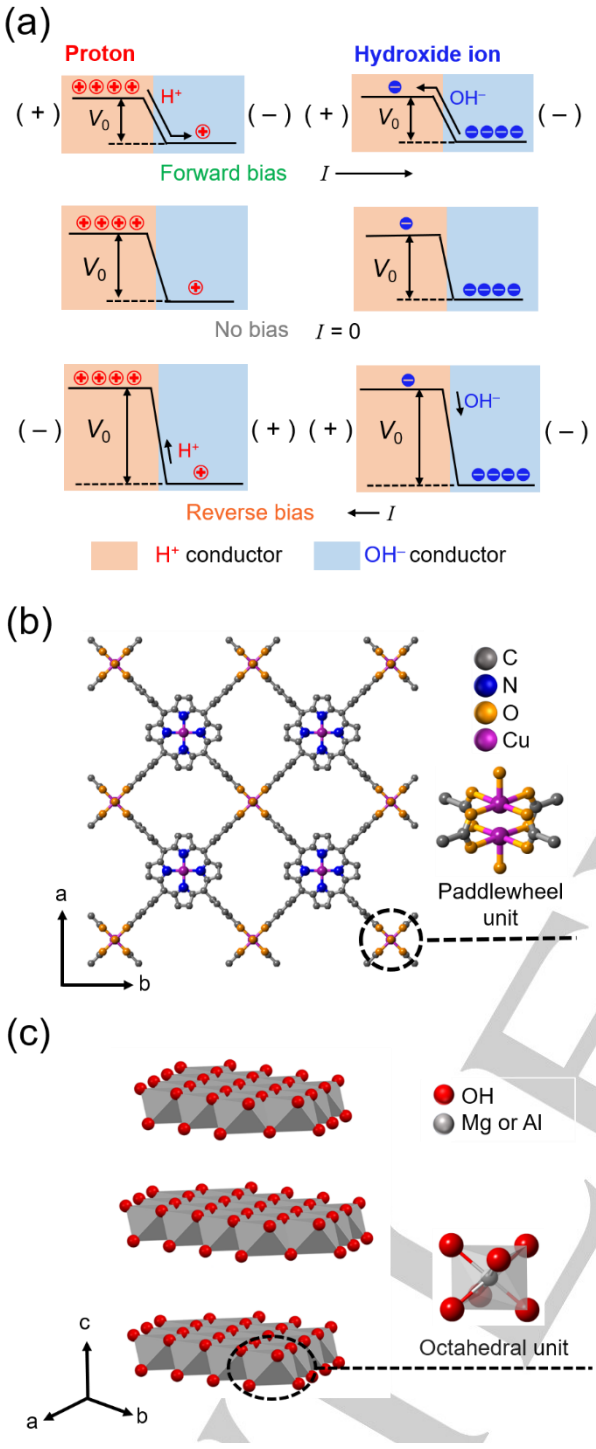


**Figure 1.** (a) Changes in potential ($V_0$) in $H^+$ and $OH^-$ in a heterogeneous membrane by applying forward and reverse bias voltages. (b) 2D sheet structure of $Cu_2$(CuTCPP). (c) Layered structure of Mg-Al-LDH($NO_3$).

which facilitates the integration of solvent-free rectifier devices without the risk of liquid leakage. Our device demonstrated an ion rectification rate (i.e., the ratio of the forward/reverse bias currents) greater than 200, which is the highest among the reported all-solid-state $H^+$–$OH^-$ rectifiers.

## Results and Discussion

Purple crystalline $Cu_2$(CuTCPP) nanosheets were obtained through a solvothermal reaction as reported previously (see Supporting Information for details).[15c] The infrared absorption spectrum showed the disappearance of the C=O stretching vibration in COOH groups at 1676 $cm^{-1}$ (Figure S2), indicating that the four carboxyl groups of CuTCPP successfully coordinate to adjacent copper ions to form dimeric copper paddlewheel units.[14] A sheet-like structure is evident in the scanning electron microscope (SEM) image with a lateral dimension of approximately 3 μm (Figure 2a). The transmission electron microscope (TEM) image of $Cu_2$(CuTCPP) deposited by dropping the ethanol suspension onto a carbon-coated copper substrate exhibited a nanosheet-like morphology (Figure S5). Because the $Cu_2$(CuTCPP) nanosheets are well dispersed in ethanol, the ethanol suspension was filtered through a polyvinylidene difluoride (PVDF) membrane filter to yield a highly oriented membrane (see Supporting Information for details). The membrane with good flexibility (Figure S6) was readily peeled from the filter after drying at 50 °C (Figure 2b). Thicknesses ranging from tens to hundreds of micrometers can be controlled using different amounts of $Cu_2$(CuTCPP) suspension. The cross-sectional SEM image (Figure 2c) showed that the membrane is formed by stacking the nanosheets, which is consistent with the SEM image of the membrane surface (Figure S7). Figure 2d shows the out-of-plane and in-plane X-ray diffraction (XRD)

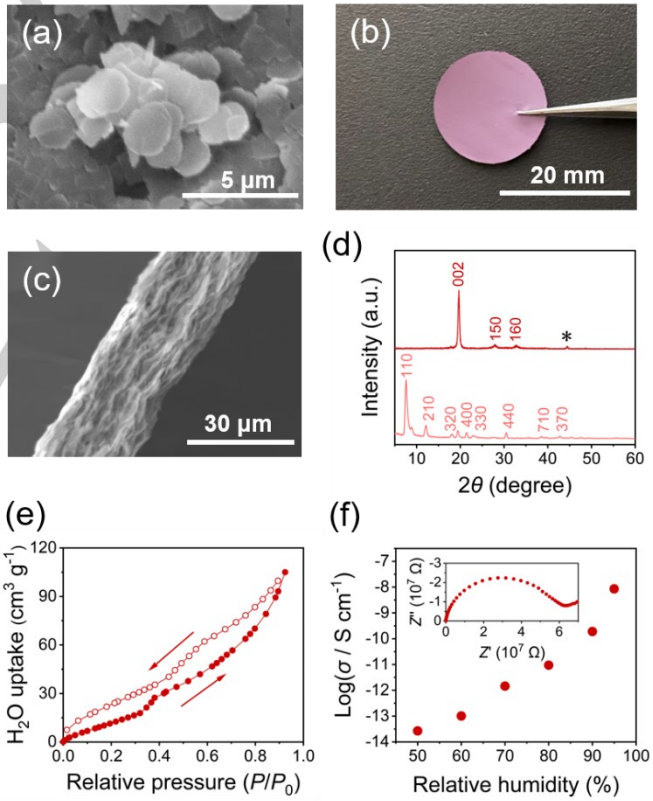


**Figure 2.** (a) Scanning electron microscope (SEM) image of $Cu_2$(CuTCPP) nanosheets. (b) Photograph of $Cu_2$(CuTCPP) free-standing membrane. (c) SEM image of the cross-section of the $Cu_2$(CuTCPP) membrane. (d) Out-of-plane (red) and in-plane (pale red) X-ray diffraction (XRD) patterns of the $Cu_2$(CuTCPP) membrane (an asterisk denotes the peak from Si substrate). (e) Water vapor adsorption (closed circles) and desorption (open circles) isotherms of the pulverized $Cu_2$(CuTCPP) membrane at 298 K. (f) Proton conductivity ($\sigma$) of the $Cu_2$(CuTCPP) membrane at 25 °C under various RH conditions (inset: Nyquist plot under 90% RH).

patterns of the membrane. In contrast to the in-plane pattern, the out-of-plane pattern is dominated by an interlayer (002) reflection, indicating the preferred orientation of the membrane along the crystallographic *c* axis. The interlayer distance of 0.45 nm is approximately similar to that reported previously.[15a, 15c]

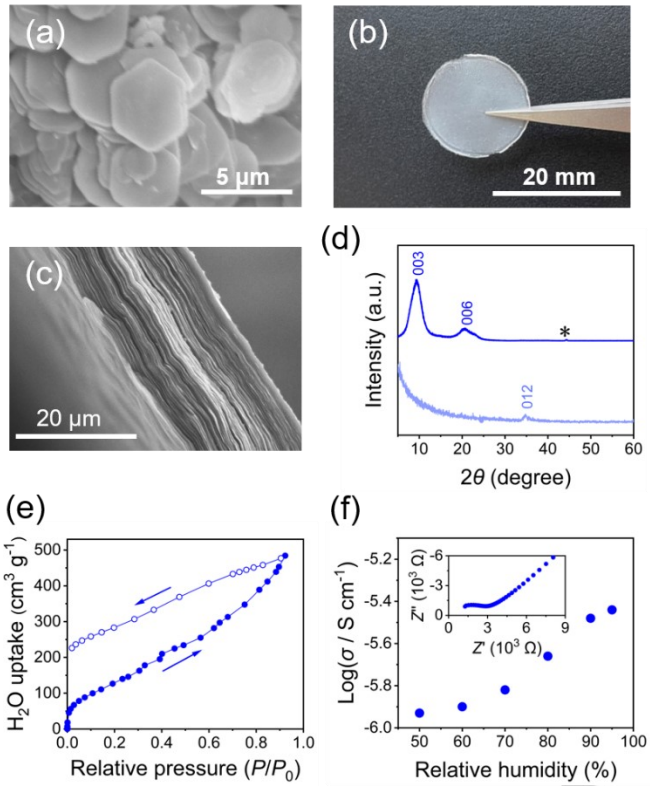


**Figure 3.** (a) SEM image of Mg-Al-LDH($NO_3$) nanosheets. (b) Photograph of Mg-Al-LDH($NO_3$) free-standing membrane. (c) SEM image of the cross-section of the Mg-Al-LDH($NO_3$) membrane. (d) Out-of-plane (blue) and in-plane (pale blue) XRD patterns of the Mg-Al-LDH($NO_3$) membrane (an asterisk denotes the peak from Si substrate). (e) Water vapor adsorption (closed circles) and desorption (open circles) isotherms of the pulverized Mg-Al-LDH($NO_3$) membrane at 298 K. (f) Proton conductivity ($\sigma$) of the Mg-Al-LDH($NO_3$) membrane at 25 °C under various RH conditions (inset: Nyquist plot under 90% RH).

Similarly, a white membrane of Mg-Al-LDH($NO_3$) ($NO_3^-$ as a counterion in the interlayer space) was obtained by filtering the formamide suspension of the nanosheets with a regular hexagonal platelet morphology (lateral dimension of approximately 4 μm),[20] as observed by SEM (Figure 3a) and TEM (Figure S5) images (see Supporting Information for details). The membrane, which also exhibited good flexibility (Figure S6), was readily peeled off from the PVDF filter after heating at 60 °C (Figure 3b). The cross-sectional SEM image confirmed that the nanosheets are well oriented in a parallel fashion (Figure 3c), as evidenced by the (00l) reflections in the out-of-plane XRD pattern (Figure 3d). Water vapor sorption isotherms of the membranes were measured to characterize their water adsorption behavior. As shown in Figures 2e and 3e, $Cu_2$(CuTCPP) and Mg-Al-LDH($NO_3$) membranes have high water vapor adsorption capacities of 105 and 484 $cm^3\ g^{-1}$, respectively, at $P/P_0$ = 0.92. There is no saturated adsorption platform, possibly owing to the irregular pore structures.[20] The sorption isotherm hysteresis observed in Mg-Al-LDH($NO_3$) may reflect the possible chemisorption of water as described above.[19] As shown in Figure 2f, the out-of-plane proton conductivity of the $Cu_2$(CuTCPP) membrane, which was measured by the a.c. impedance method, considerably increases with increasing humidity. This must be a reflection of the concentration of water in the pores, which can serve as hopping sites for protons originating from the uncoordinated carboxylic groups (Figure S1).[22] The Mg-Al-LDH($NO_3$) membrane also showed humidity-dependent proton conductivity (Figure 3f); however, the conductivity change is less pronounced than that of the $Cu_2$(CuTCPP) membrane. The presence of hydroxyl groups at higher concentrations than the proton species in $Cu_2$(CuTCPP) appears to be a part of the reason for humidity-independent conduction.

To investigate unidirectional ion conduction in the membranes, we performed d.c. resistivity measurements using Pd plates as electrodes at 25 °C and 90% RH. As shown in Figures 4a and 4b, a nearly linear and symmetric current-voltage (*I*–*V*) plot was observed when only one of the membranes, i.e., $Cu_2$(CuTCPP) or Mg-Al-LDH($NO_3$), was sandwiched by the electrodes. Specifically, both membranes exhibited apparent relaxation behavior (Figure S12) and significantly reduced the current under dry conditions (30% RH; Figures 4a and 4b). These results provide firm evidence that ions (i.e., protons and hydroxide ions) instead of electrons are responsible for the observed current in such membranes.

The mechanical combination of the two membranes led to the drastic change in the *I*–*V* curve. As demonstrated in Figure 4c, the heterogeneous membrane displayed a nonlinear and asymmetric *I*–*V* curve, where the forward bias current starts to increase at around 1.0 V. The highly rectified ion transport (623 μA at a forward bias voltage of +10 V and –2.1 μA at a reverse bias voltage of –10 V) clearly indicates unidirectional proton and hydroxide ion transport in the heterogeneous membrane. The proton rectification ratio (PRR), defined as the ratio of the forward/reverse bias current at ±10 V, was estimated to be as high as 297. We also characterized unidirectional proton/hydroxide ion conduction by applying constant positive and negative d.c. voltages to the heterogeneous membrane. Figure 4d clearly demonstrates that the current becomes almost constant after applying a voltage of ±10 V for approximately 10 s in both the forward and reverse directions. The mechanism of the continuous supply of protons and hydroxide ions will be discussed later. It should be noted that the PRR value estimated from the currents in the stable region (approximately 292) is in good agreement with that estimated based on the *I*–*V* curve.

To assess the cyclability and reproducibility of the rectification performance, *I*–*V* measurements were conducted several times at intervals of several hours for seven different sets of heterogeneous membranes. A typical temporal variation of the PRR is shown in Figure 4e. The first scan yielded a very high PRR value (344), as shown in Figure 4c; however, the value suddenly dropped to 59 in the second scan and remained fairly constant (50–82) in the following scan. Given that the membranes demonstrated a significant increase in the reverse bias current while maintaining the forward bias current in the second scan (Figure 4f), the fall-off of the PRR possibly arises from the generation of water in the interfacial region between the $Cu_2$(CuTCPP) and Mg-Al-LDH($NO_3$) membranes during the first scan, owing to the association of migrated protons and hydroxide ions. Actually, we observed water streaks at the interface between the membranes after the experiments, which were invisible in the

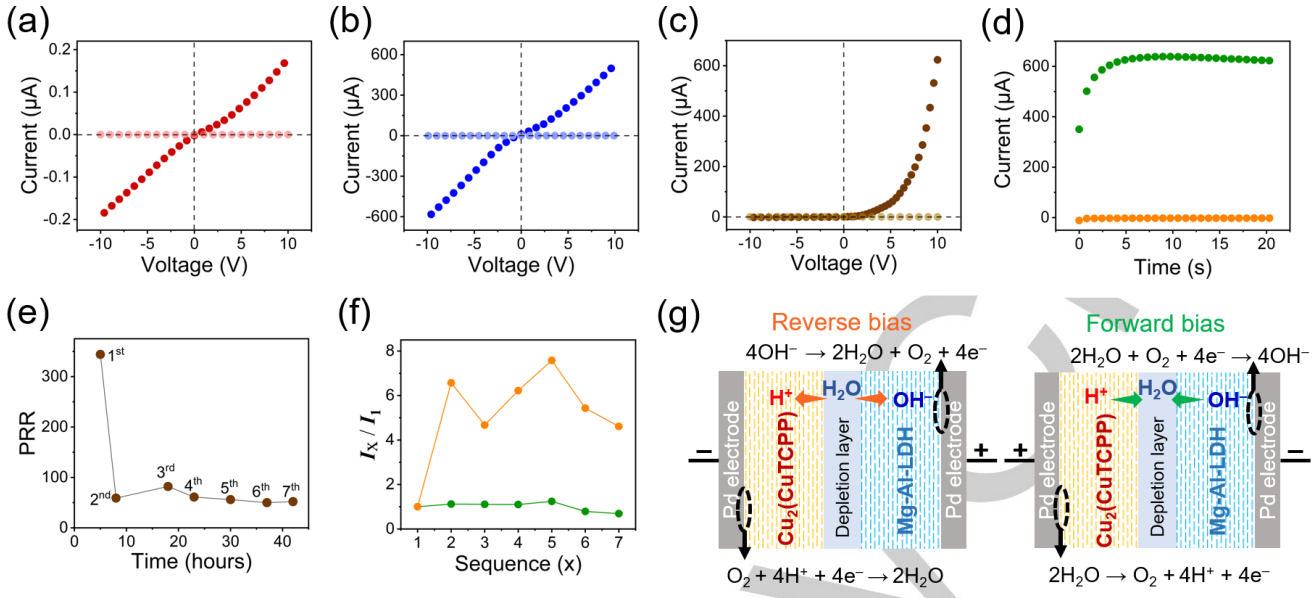


**Figure 4.** *I–V* plots of single membranes of (a) $Cu_2$(CuTCPP) and (b) Mg-Al-LDH($NO_3$) at 25 °C under 30% RH (pale red/blue circles) and 90% RH (red/blue circles). (c) *I–V* plot of $Cu_2$(CuTCPP)/Mg-Al-LDH($NO_3$) heterogeneous membrane at 25 °C under 30% RH (pale brown circles) and 90% RH (brown circles). (d) Time dependence of current of the heterogenous membrane under applied voltages of +10 V (forward bias; green circles) and –10 V (reverse bias; orange circles). (e) Sequence-dependent proton rectification ratio (PRR) of the heterogenous membrane. (f) Relative forward (green circles) and reverse currents (orange circles) as a function of the number of scans (x) with respect to those in the first scan ($I_x$ / $I_1$). (g) Schematics of ion generation in the heterogeneous membrane under reverse and forward bias conditions.

heterogeneous membrane placed at 25 °C under 90% RH for 2 days without applying a bias voltage (Figure S13). The generation of water molecules consequently increases the reverse bias current because of the increased ion carrier concentration via water dissociation.[3b] A similar behavior was observed in the other six heterogeneous membranes, as shown in Figure S15 and Table S1, where the PRR values after the second scan lie in the range of 40–80. We note that five out of seven heterogeneous membranes presented a PRR value higher than 200 in the first scan, although the value varied considerably between the samples (35–922). The PXRD measurements revealed that the structure of each membrane was mostly intact during the rectification experiments (Figure S16).

As mentioned above, the operating principles of proton rectifiers are analogous to those of p–n diodes (Figure 1a). Because considerable amounts of protons and hydroxide ions are accommodated in the $Cu_2$(CuTCPP) and Mg-Al-LDH($NO_3$) membranes, respectively, the resulting pH gradient promotes the diffusion of protons in the $Cu_2$(CuTCPP) membrane and hydroxide ions in the Mg-Al-LDH($NO_3$) membrane toward the interfacial region, even under no applied voltage. The recombination of protons and hydroxide ions generates water, and the neutralized interfacial region (termed as the depletion layer) leads to current ceasing. Applying a forward bias voltage (i.e., $Cu_2$(CuTCPP) facing the anode) further promotes the ion diffusion of both protons and hydroxide ions toward the interfacial region, which is a factor dominating the observed current. The water electrolysis reactions at the boundary between the membrane and Pd electrode, i.e., water oxidation ($2H_2O \rightarrow O_2 + 4H^+ + 4e^-$) on the anode side and reduction on the cathode side ($2H_2O + O_2 + 4e^- \rightarrow 4OH^-$), presumably occur continuously to supply protons and hydroxide ions to the membranes (right panel of Figure 4g). In the opposing mode (i.e., $Cu_2$(CuTCPP) facing the cathode), the reverse bias increases the potential barrier for both protons and hydroxide ions, which suppresses ion diffusion driven by the concentration gradients. Eventually, protons and hydroxide ions are directed toward the cathode and anode sides, respectively. In the reverse bias mode, the dissociation of water accommodated in the interfacial region possibly generates protons and hydroxide ions (left panel of Figure 4g). The reverse bias current must be significantly low because of the low dissociation rate despite the generation of water in the interfacial region during the first scan, which appears to increase the reverse bias current.

To date, a few all-solid-state $H^+$–$OH^-$ rectifier devices have been fabricated using heterogeneous junctions of proton-conducting and hydroxide ion-conducting membranes. An early example is the work of Seno and Yamabe in 1964; acid- and base-washed ion-exchange resins were used after soaking in water (water weight: 56%). They demonstrated that a PRR value of approximately 100 was attained in a humidity-controlled chamber.[9a] In 2013, Rolandi et al. reported the rectifying behavior of a heterogeneous membrane composed of maleic and proline chitosan films, which presented a PRR value less than 10 under 75% RH and 5% $H_2$ gas atmosphere.[9d] It should be noted that our all-solid-state $H^+$–$OH^-$ rectifier device mainly demonstrates three advantages over those in the previous studies: (1) high rectification ratio (PRR > 200), (2) high designability, and (3) well-defined structure of the device components. In addition, the facile operating conditions (i.e., 90% RH), without soaking in water prior to the performance or using flammable $H_2$ gas, render it particularly suitable for several practical applications. Notably, both membranes used in this study remained intact upon prolonged immersion in water (Figure S17). Chemical characteristics of PCPs, such as proton concentration (i.e., p$K_a$), proton mobility, and hydrophilicity/hydrophobicity, can be modified by selecting metal ions and organic linkers while maintaining the basic framework structure.[13] Given that their structures can be evaluated appropriately by diffraction techniques in contrast to the organic

polymers used in earlier studies, the present system is evidently a promising platform for studying the structure–property relationship to develop all-solid-state $H^+$–$OH^-$ rectifiers.

## Conclusion

In conclusion, we fabricated an all-solid-state proton rectifier by the facile mechanical lamination of two free-standing membranes; namely, a proton-conducting PCP, $Cu_2$(CuTCPP), and hydroxide ion-conducting LDH, Mg-Al-LDH($NO_3$). The *I–V* characteristics provide a rectification ratio as high as > 200 at 25 °C under 90% RH, which is the highest recorded value. In addition to the remarkable performance under electrolyte-free conditions, the present heterogeneous membrane has the potential to modify and control the water permeability, $H^+$/$OH^-$ mobility, and p$K_a$ in the pores, which noticeably affect the rectifying behavior, by selecting components such as metal ions and organic linkers. These results will open the way for the exploration of new and more advanced all-solid-state proton rectifiers through rational design. Studies along this line are in progress.

## Acknowledgements

This work was supported by the ACCEL program (JPMJAC1501) of the Japan Science and Technology Agency (JST) and JSPS KAKENHI (Grant Nos. 20H02708 and 20H05623).

## Conflict of Interest

The authors declare no conflict of interest.

## Data Availability Statement

The data that support the findings of this study are available from the corresponding author upon reasonable request

**Keywords:** porous coordination polymer (PCP) • layered double hydroxide • all-solid-state • proton rectification • rectifier device

[1] a) H. C. Blair, S. L. Teitelbaum, R. Ghiselli, S. Gluck, *Science* **1989**, *245*, 855-857; b) G. Steinberg-Yfrach, J. L. Rigaud, E. N. Durantini, A. L. Moore, D. Gust, T. A. Moore, *Nature* **1998**, *392*, 479-482; c) D. Gadsby, *Nat. Rev. Mol. Cell Biol.* **2009**, *10*, 344-352.

[2] a) D. Gust, T. A. Moore, A. L. Moore, *Acc. Chem. Res.* **2001**, *34*, 40-48; b) P. K. Ghosh, A. Y. Smirnov, F. Nori, *J. Chem. Phys.* **2009**, *131*, 035102; c) S. Berardi, S. Drouet, L. Francàs, C. Gimbert-Suriñach, M. Guttentag, C. Richmond, T. Stoll, A. Llobet, *Chem. Soc. Rev.* **2014**, *43*, 7501-7519; d) S. Chabi, K. M. Papadantonakis, N. S. Lewis, M. S. Freund, *Energy Environ. Sci.* **2017**, *10*, 1320-1338.

[3] a) Y. Tanaka, *Membr. Sci. Tech.* **2007**, *12*, 405-436; b) R. Pärnamäe, S. Mareev, V. Nikonenko, S. Melnikov, N. Sheldeshov, V. Zabolotskii, H. V. M. Hamelers, M. Tedesco, *J. Membr. Sci.* **2021**, *617*, 118538.

[4] K. Jiao, J. Xuan, Q. Du, Z. Bao, B. Xie, B. Wang, Y. Zhao, L. Fan, H. Wang, Z. Hou, S. Huo, N. P. Brandon, Y. Yin, M. D. Guiver, *Nature* **2021**, *595*, 361-369.

[5] W. Guo, Y. Tian, L. Jiang, *Acc. Chem. Res.* **2013**, *46*, 2834-2846.

[6] B. Lovrecek, A. Despic, J. O. M. Bockris, *J. Phys. Chem.* **1959**, *63*, 750-751.

[7] a) P. K. Giesbrecht, M. S. Freund, *Chem. Mater.* **2020**, *32*, 8060-8090; b) Z. Zhang, X. Y. Kong, K. Xiao, Q. Liu, G. Xie, P. Li, J. Ma, Y. Tian, L. P. Wen, L. Jiang, *J. Am. Chem. Soc.* **2015**, *137*, 14765-14772.

[8] a) Z. Siwy, A. Fuliński, *Am. J. Phys.* **2004**, *72*, 567-574; b) L. J. Cheng, L. J. Guo, *Chem. Soc. Rev.* **2010**, *39*, 923-938.

[9] a) M. Seno, T. Yamabe, *Bull. Chem. Soc. Jpn.* **1964**, *37*, 668-671; b) J. J. Langer, *Appl. Phys. A* **1984**, *34*, 195-198; c) J. J. Langer, M. Martyński, *Adv. Opt. Mater.* **1999**, *9*, 15-18; d) Y. Deng, E. Josberger, J. Jin, A. F. Roudsari, B. A. Helms, C. Zhong, M. P. Anantram, M. Rolandi, *Sci. Rep.* **2013**, *3*, 2481.

[10] a) A. Schoedel, M. Li, D. Li, M. O'Keeffe, O. M. Yaghi, *Chem. Rev.* **2016**, *116*, 12466-12535; b) L. Feng, K. Y. Wang, G. S. Day, H. C. Zhou, *Chem. Soc. Rev.* **2019**, *48*, 4823-4853; c) S. Kitagawa, R. Matsuda, *Coord. Chem. Rev.* **2007**, *251*, 2490-2509.

[11] a) K. D. Kreuer, *Chem. Mater.* **1996**, *8*, 610-641; b) *Proton Conductors: Solids, Membranes and Gels–Materials and Devices*, (Ed.: P. Colomban), Cambridge University Press, Cambridge, **1992**.

[12] a) D. Zhao, D. J. Timmons, D. Yuan, H. C. Zhou, *Acc. Chem. Res.* **2011**, *44*, 123-133; b) M. Y. Masoomi, A. Morsali, A. Dhakshinamoorthy, H. Garcia, *Angew. Chem. Int. Ed.* **2019**, *58*, 15188-15205, *Angew. Chem* **2019**, *131*, 15330-15347; c) A. Kirchon, L. Feng, H. F. Drake, E. A. Joseph, H. C. Zhou, *Chem. Soc. Rev.* **2018**, *47*, 8611-8638; d) A. E. Baumann, D. A. Burns, B. Liu, V. S. Thoi, *Commun. Chem.* **2019**, *2*, 86; e) H. D. Lawson, S. P. Walton, C. Chan, *ACS Appl. Mater. Interfaces* **2021**, *13*, 7004-7020; f) W. Lu, Z. Wei, Z. Y. Gu, T. F. Liu, J. Park, J. Park, J. Tian, M. Zhang, Q. Zhang, T. Gentle III, M. Bosch, H. C. Zhou, *Chem. Soc. Rev.* **2014**, *43*, 5561-5593; g) R. Freund, O. Zaremba, G. Arnauts, R. Ameloot, G. Skorupskii, M. Dincă, A. Bavykina, J. Gascon, A. Ejsmont, J. Goscianska, M. Kalmutzki, U. Lächelt, E. Ploetz, C. S. Diercks, S. Wuttke, *Angew. Chem. Int. Ed.* **2021**, *60*, 23975-24001, *Angew. Chem.* **2021**, *133*, 24174-24202; h) N. Stock, S. Biswas, *Chem. Rev.* **2012**, *112*, 933-969; i) J. Li, P. M. Bhatt, J. Li, M. Eddaoudi, Y. Liu, *Adv. Mater.* **2020**, *32*, 2002563.

[13] D. W. Lim, H. Kitagawa, *Chem. Rev.* **2020**, *120*, 8416-8467.

[14] R. Makiura, S. Motoyama, Y. Umemura, H. Yamanaka, O. Sakata, H. Kitagawa, *Nat. Mater.* **2010**, *9*, 565-571.

[15] a) G. Xu, T. Yamada, K. Otsubo, S. Sakaida, H. Kitagawa, *J. Am. Chem. Soc.* **2012**, *134*, 16524-16527; b) G. Xu, K. Otsubo, T. Yamada, S. Sakaida, H. Kitagawa, *J. Am. Chem. Soc.* **2013**, *135*, 7438-7441; c) M. Tian, F. Pei, M. Yao, Z. Fu, L. Lin, G. Wu, G. Xu, H. Kitagawa, X. Fang, *Energy Storage Mater.* **2019**, *21*, 14-21; d) G. D. Wu, H. L. Zhou, Z. H. Fu, W. H.Li, J. W. Xiu, M. S. Yao, Q. H. Li, G. Xu, *Angew. Chem. Int. Ed.* **2021**, *60*, 9931-9935, *Angew. Chem.* **2021**, *133*, 10019-10023.

[16] a) X. Huang, Z. Zeng, H. Zhang, *Chem. Soc. Rev.* **2013**, *42*, 1934-1946; b) H. Zhang, Z. H. Fu, D. Legut, T. C. Germann, R. F. Zhang, *RSC Adv.* **2017**, *7*, 55912-55919.

[17] K. H. Goh, T. T. Lim, Z. Dong, *Water Res.* **2008**, *42*, 1343-1368.

[18] a) P. Sun, R. Ma, X. Bai, K. Wang, H. Zhu, T. Sasaki, *Sci. Adv.* **2017**, *3*, e1602629; b) Y. Furukawa, K. Tadanaga, A. Hayashi, M. Tatsumisago, *Solid State Ionics* **2011**, *192*, 185-187; c) L. Li, R. Ma, Y. Ebina, N. Iyi, T. Sasaki, *Chem. Mater.* **2005**, *17*, 4386−4391.

[19] P. Sun, F. Chen, W. Zhou, X. Liu, R. Ma, T. Sasaki, *Mater. Horiz.* **2019**, *6*, 2087-2093.

[20] D. G. Evans, X. Duan, *Chem. Commun.* **2006**, *5*, 485-496.

[21] M. Thommes, K. Kaneko, A. V. Neimark, J. P. Olivier, F. Rodriguez-Reinoso, J. Rouquerol, K. S. W. Sing, *Pure Appl. Chem.* **2015**, *87*, 1051-1069.

[22] Y. N. Zhou, L. L. Liu, Q. W. Liu, X. X. Liu, M. Z. Feng, L. Wang, Z. G. Sun, Y. Y. Zhu, X. Zhang, C. Q. Jiao, *Inorg. Chem.* **2021**, *60*, 17303-17314.

## Entry for the Table of Contents

Insert graphic for Table of Contents here.

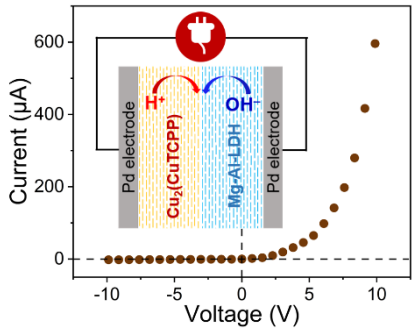


An all-solid-state proton rectifier was fabricated using a heterogeneous membrane composed of proton-conducting coordination polymer, $Cu_2$(CuTCPP), and hydroxide ion-conducting layered double hydroxide, Mg-Al-LDH($NO_3$). The device demonstrated a proton rectification ratio greater than 200, which is the highest among the reported all-solid-state $H^+$–$OH^-$ rectifiers.